This article has been accepted for publication in a future issue of this journal, but has not been fully edited. Content may change prior to final publication. Citation information: DOI 10.1109/TTHZ.2020.2985642, IEEE Transactions on Terahertz Science and Technology

Quasi-Optical Sub-THz Circular Dichroism Spectroscopy of solvated Myoglobin

Jhih-Hong Cheng [1], Robert C. Jones [1], Oleksandr Sushko [2], Yumiko Tashiro[3], and Robert Donnan[1]

[1]School of Electronic Engineering and Computer of Science, Queen Mary, University of London, London, UK
[2] Radioengineering Department Igor Sikorsky Kyiv Polytechnic institute, Kyiv, Ukraine
[3]School of Biological and Chemical Sciences, Queen Mary, University of London, London, UK
Email: j.cheng@qmul.ac.uk, r.c.jones@qmul.ac.uk, o.y.sushko@gmail.com, y.tashiro@qmul.ac.uk, r.donnan@qmul.ac.uk

***Abstract*— A quasi-optially-based, sub-terahertz (sub-THz), circular dichroism (CD) spectrometer is demonstrated on the model protein, myoglobin, over waveguide bands D (110 – 170 GHz) and H (220 – 325 GHz). In so doing, an equivalent methodology is propounded for acquiring cross-polar spectra that eliminates the need for having to physically rotate the receive-horn through 90˚. A significant source of systematic-error is thereby eliminated (and, no less, random-error, that follows when cabling is moved). The 'zero-crossing' points of CD spectra are characterized as they are correlated with traditional far-UV CD spectra for given environmental parameter settings of, for example, pH and/or sample concentration.**

***Index Terms*—Terahertz; Circular Dichroism; Quasi-optical; Myoglobin;**

I. Introduction

Terahertz (THz) light is located between the microwave and infrared wavelength bands of the electromagnetic spectrum. It is conventionally given to span from 300 GHz to 10 THz (associated wavelengths being 1 to 0.03 mm) [1, 2]. Sub-THz spectroscopy (spanning 100 to 300 GHz) is here undertaken via quasi-optical (QO) circuits. Millimeter – to – sub-millimeter wavelength electromagnetic radiation has a spatiotemporal scale that efficiently couples to protein vibrational modes [3,4] and dielectric water relaxation [11-13] fundamental to manifold chemical and physical processes such as those active in the hydration dynamics of biological molecules [7, 8]. Its cognate medical applications, specifically, are summarised by Speigel et al [5] and Pickwell et al [6].

Normal biological molecular processes are such that they occur at 'room' temperature, energy being drawn from the thermal bath in which they are immersed. Room temperature (i.e. NTP), equates to $k_B T|_{20^\circ C} \sim 6\ kcal.mol^{-1}$; k_B having its conventional meaning as Boltzmann's constant. This thermal energy has an associated Blackbody spectrum peaking at ~ 30 THz (FWHM approximately bounded between 16 and 50 THz). THz modes are coming to be regarded as fundamental drivers to structural biological action, such as folding [7]. The dynamics of biomolecule, such as proteins, can be studied via a normal modes' analysis. The larger the biomolecule, the lower the frequency of the lowest mode. Such low frequency THz modes play a key role in protein folding [8, 9]. The study of such modes, to be of physiological relevance, is best done for solvated proteins. Water, however, is well known to cause heavy attenuation of propagating electromagnetic radiation; its specific attenuation at 1 THz is 180 dB.mm^{-1}. Because of this strong absorption, most research of dissolved proteins in recent years has focused on the variation in absorption coefficients at different concentration [7, 10-17] and in structural changes at different temperatures [8, 16, 17]. Studies on the influence of the hydration layer enveloping proteins or on dynamic hydrogen bonding in liquids have also increased significantly recently [10, 11, 17]. A theory as to why the absorption coefficient of a liquid sample changes with temperature variation, is attributed to the complex dynamics of the water molecule. Water rotational relaxation is the dominant mechanism influencing absorption rate [11-13].

In earlier studies with THz spectroscopy, such as THz time-domain spectroscopy (THz TDS), biological samples were mostly used in the form of dried powder to avoid strong water absorption [18]. While water exhibits high THz absorption, it remains essential in organizing the structure of a biomolecule, i.e. in helping proteins to obtain their folded, functional state [19]. According to Singh et al [20], the backbone of a protein is no longer well-defined at lower hydration levels, indicating that a protein sample must be hydrated to at least 30% of its total weight. Water forms a hydrogen bonding network surrounding the protein, and the coupling between protein and hydration-water by H-bonding triggers strong interactions [20, 21]. Thus, H-bonding plays a critical role in protein folding, stabilization of protein conformation, and protein dynamics. Significantly, the water molecule is not optically active, while the bio-molecule is. Optical CD is widely used to study the secondary conformational forms of protein and these respond differently to different polarizations of light at optical wavelengths. THz CD seeks to sense for expected secondary conformational activity at longer wavelengths. CD is a direct means for studying the dynamics of solvated proteins and it is particularly implemented as described here by means of an analyzing quasi-optical circuit driven by a vector network analyzer (VNA). The VNA supplies the necessary detection sensitivity to compensate for the heavy signal attenuation by water.

Biological polymers, such as amino acids, peptides, proteins and higher structural levels of biopolymers (DNA and RNA) that are folded into larger structures all exhibit chirality. CD is the difference in absorption between left- and right-handed circularly-polarized light, and such phenomena occur in molecules containing chiral chromophores. CD

spectroscopy has longstanding application in studying biomolecules with optical light, particularly in the ultra-violet (UV) [22]. The far UV CD spectroscopy is widely use to study folding and unfolded states of polypeptides and proteins [22-26]. The far UV CD spectrum (190-250 nm) of proteins reveals characteristic features of their so-called 'secondary structure'. The chromophore is the peptide bond that influences the absorption level below 240 nm [23-26]. Different types of protein secondary structure are identified by their characteristic CD UV absorption 'fingerprint'. For the tertiary structure of proteins, the near UV CD spectrum provides a valuable fingerprint for identification and categorization of wild-type and mutant proteins [22, 27]. For the aromatic amino acids, their spectra is most rich in the near UV CD region (260 to 320 nm). Infrared (IR) light has been utilized in Vibrational Circular Dichroism (VCD) to study the 3D framework of small organic molecules (protein, DNA, nucleic acids, or peptides) [28, 29]. THz CD techniques have been used to study biomaterial and chiral material [30, 31]. For amino acids, proteins, and other biological molecules that are chiral, any protein that has helical secondary structure is expected to have THz CD signature. THz CD is especially sensitive to the secondary structures of proteins, enabling it to differentiate close variants in biological signature among different biomolecules. As chiral objects, biological polymers present strong absorption to THz light by large-amplitude, collective vibrational modes [32]. Some THz vibrational CD spectroscopies have been developed to study biomolecules [30, 33] and the molecular dynamics of peptides [34].

Implementing THz spectroscopies typically depends on a high-power laser (e.g. THz time-domain spectroscopy and THz Raman spectroscopy). These THz CD spectroscopies further require signal conditioning schemes to transform from linear – to – circular polarization before irradiating the sample under test. Optical path-length needs to be preserved between sample-versus-reference (background) scans. This typically depends upon a physical enclosure of the THz signal path to maintain a dry (non-absorbing) atmosphere, free of convective turbulence. We report a simpler apparatus. Sub-THz CD is effected by a quasi-optical (QO) circuit that is driven by a four-port Agilent PNA-X vector network analyzer (N5244A). Extremely low-loss is the biggest advantages of Gaussian beam optics. The QO scheme supports contiguous waveguide-band coverage from 0.05 – 1.1 THz and the VNA affords MHz to kHz-level spectral resolution. (The authors have a frequency span of 105 GHz, and the VNA can support a maximum of circa 160k frequency points, which affords kHz resolution). As will be described in section B below, the benefit of implementing THz CD via QOs lies in the hard and fixed, machined-in accuracy to high-precision tolerances, of optical shaped-surfaces and inter-component path lengths; control of orthogonality of transmit and receive polarization states and the kinematic repeatability with which signal-conditioning components, such as wire-grid polarizers and Faraday plates, can be introduced and removed from the circuit to achieve linear – to – circular analysis [35, 36]. To eliminate systematic errors and to receive more phase-stable data, measurements by scheme 1 (involving traditional cross-polar acquisition), and scheme 2 (employing a 45° wire-grid polarizer), will be compared in section B.

II. EXPERIMENTAL METHODS

A. Sample preparation

The protein Myoglobin (MB) from the equine skeletal muscle was chosen as a model system for demonstration of THz-CD. Lyophilized powder of MB with a purity of 95 to 100% was purchased from Sigma Aldrich and used without any further treatment.

20 mM phosphate buffer (K_2HPO_4 /KH_2PO_4) was chosen as the dissolving solution. By mixing K_2HPO_4 and KH_2PO_4, 1 M of phosphate buffer of pH 8.26 (98ml/2ml), pH 7 (61.5ml/38.5ml), and pH 5.5 (3.5ml/96.5ml) were obtained. All three buffers were verified by a pH meter after mixing and adjusted by adding the appropriate volume of K_2HPO_4 and KH_2PO_4 to achieve the required pH value. Double-distilled water was used to prepare a sequence of buffers from 1 M to 20 mM. The first system studied was 10 mg of MB dissolved in 2 mL of 20 mM phosphate buffer at three pH values (8.26, 7, 5.5) without any further purification. To reduce manual error, different pH values of MB solutions were diluted to 1 mg/ml and 0.25 mg/ml in separate tubes. MB has been extensively studied by IR, visible, UV and x-ray light. In THz range, the absorption spectra and dielectric properties of MB are studied well [11, 37-39]. Fig. 1 shows the 3D structure of the equine Myoglobin. The green ribbon is the backbone consisting of α-helices to which side chains and other residues are connected. The red structure represents a heme group.

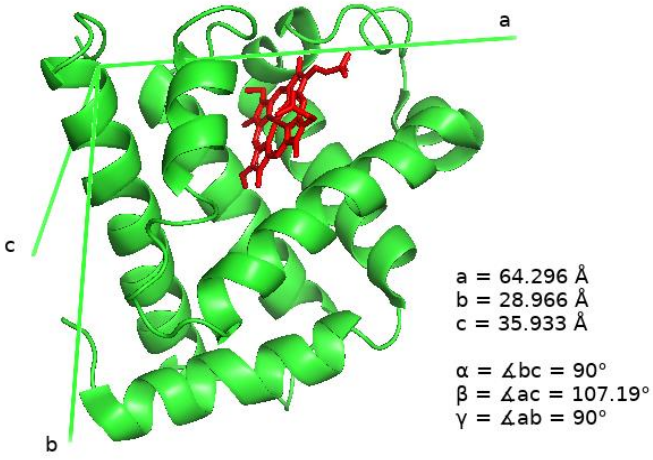

Figure 1: The 3D structure of Myoglobin, form equine skeletal muscle, is shown to have monoclinic crystal structure. The green ribbon represents the `backbone` of the molecule and the red structure represents a heme group.

B. THz circular dichroism quasi-optical system

The VNA-driven QO THz CD spectrometer was configured as shown in Fig. 2. The VNA has a 10 MHz to 43.5 GHz baseband and with pairs of transmitting and receiving frequency-multiplier modules is able to extend frequency-coverage up to 1.1 THz. Transmitting and receiving frequency-multiplier modules were terminated with phase-matched, high-gain, ultra-Gaussian, corrugated horns (H_1 and H_2 in Fig. 2). An off-axis ellipsoidal mirror (F1) is set to efficiently receive the beam-field from the transmitting horn and couple it to mirror F2, one of a confocal pair with F3 at whose

common focus the sample (S) is situated. F1 and F4, have a 250 mm focal length and F2 and F3 a focal length of 100 mm.

A Bruker liquid cell was used as a sample holder at the con-focus of mirrors F2 and F3. The cell consisted of two neoprene gaskets, two TPX plates and a PTFE spacer. For each filling, 50 µL of the MB liquid was injected into the cell via a pipette. The gap (or the effective thickness of solution), inside the cell is 100 µm. A ferrite plate was introduced prior to the sample, the normal of its broad-face parallel to the beam-axis. The thickness of the plate is 2.02 mm. The function of this leading ferrite plate is to induce Faraday rotation of the vertical, linearly-polarized signal beam from the transmit horn that adds to the cross-polar transmission component (later used, with the co-polar transmission signal, to synthesise left-handed circular polarisation (LHCP) in particular [35, 40]. In CD, right-handed circular polarisation (RHCP), typically dominates over LHCP.

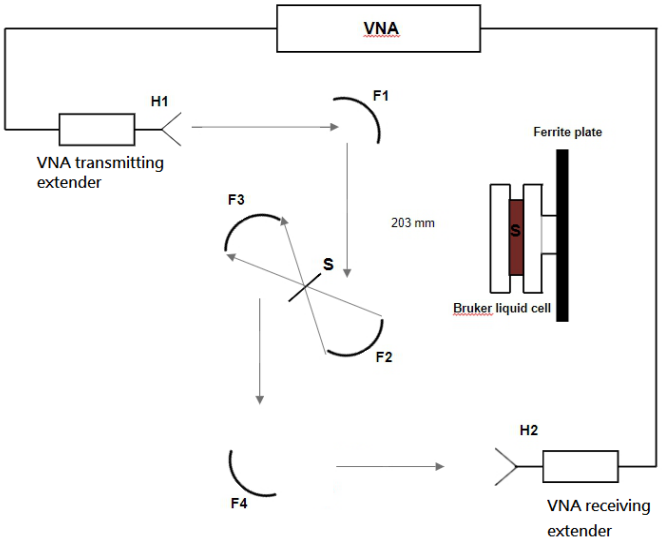

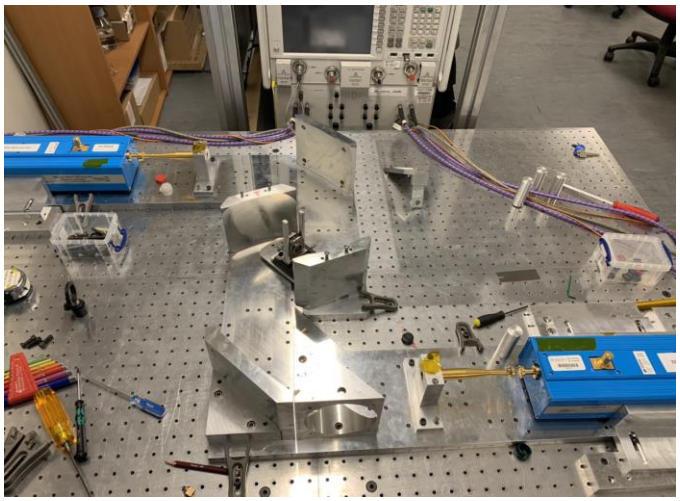

Figure 2: Schematic and photograph of the sub-THz quasi-optical apparatus and circuit for implementing circular dichroism spectroscopy. Components F1 and F4 are off-axis ellipsoidal mirrors (common focal length 250 mm; the focal length of the fast parabolic mirrors F2 and F3 is 100 mm). H1 and H2 ultra-Gaussian corrugated horns coupled to frequency extension modules.

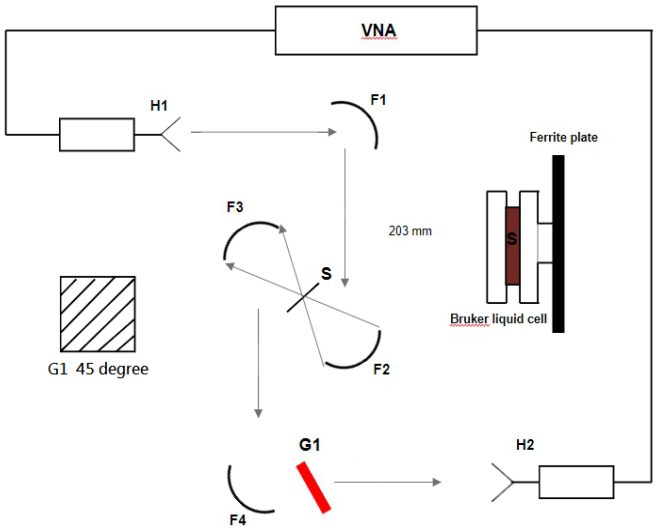

Figure 3: Schematic of Method II measurement. A 45° wire-grid polarizers G1 was introduced between F4 and H2 to measure 45° polarized signal to obtain a cross-polar signal that did not entail rotation of the receive horn.

In order then to have a workable CD signature, LHCP has this effective boost applied to it as a simple scaling factor.

In this sub-THz CD QO system, two perpendicular linear transmission signals, t_{co} and t_{cr}, were measured and used to synthesis left- and right-handed circularly polarized transmit waves. Formally then, the general elliptically-polarized wave may be expressed as

$$\vec{E} = \begin{bmatrix} E_x e^{i(2\pi\nu t)} \\ E_y e^{i(2\pi\nu t+\tau)} \end{bmatrix} = \frac{e^{i(2\pi\nu t)}}{\sqrt{E_x^2+E_y^2}} \begin{bmatrix} x \\ y e^{i\tau} \end{bmatrix} \quad (1)$$

where τ is the phase difference between linear x and y components; $x = E_x/\sqrt{E_x^2+E_y^2}$ and $y = E_y/\sqrt{E_x^2+E_y^2}$ [40]. Taking both transmission amplitudes to be identical, the normalized co- and cross-polar transmission beams can be expressed as [35, 40]:

$$\mathrm{Tcr} = \begin{bmatrix} 1 \\ 0 \end{bmatrix}$$

$$Tco = \begin{bmatrix} 0 \\ 1 \end{bmatrix}. \quad (2)$$

For x = 0, signals are linearly polarized along the y-axis, and vice versa. For obtaining right- and left-handed circular polarizations, $\tau = \pi/2$ and $3\pi/2$ are respectively substituted into (1). The standard Jones vector representation of a circularly polarized is then

$$\vec{\mathrm{E}} \equiv \frac{1}{\sqrt{2}} \begin{bmatrix} 1 \\ \pm i \end{bmatrix}. \quad (3)$$

As noted earlier, the CD spectrum is calculated based on linear co- and cross-polar signals. The equation of right- and left-handed circularly-polarized waves can be written as

This article has been accepted for publication in a future issue of this journal, but has not been fully edited. Content may change prior to final publication. Citation information: DOI 10.1109/TTHZ.2020.2985642, IEEE Transactions on Terahertz Science and Technology

$$T_+(\nu) \equiv \frac{1}{\sqrt{2}}\left(Tcr(\nu) - iTco(\nu)\right)$$

and

$$T_-(\nu) \equiv \frac{1}{\sqrt{2}}(Tcr(\nu) + iTco(\nu)). \quad (4)$$

With $T_+(\nu)$ and $T_-(\nu)$ respectively describing RHCP and LHCP, the CD spectrum $\Delta T(\nu)$ is calculated as:

$$\Delta T(\nu) = |T_+(\nu)| - |T_-(\nu)|. \quad (5)$$

C. *Measurement schemes 1 and 2*

The traditional measurement procedure of scheme I measures the cross-polar component of signal propagation in the conventional manner by rotating the receiving horn, H2. The procedure is as follows:

1. Set up the co-polar measurement as in Fig.2 without the sample and ferrite plat in position S.
2. Normalize the free-space background as shown in the reference.
3. Introduce the empty Bruker cell and re-set the background to remove interference and etalon reflections originating from the external and internal faces of the empty cell.
4. Inject liquid sample into the Bruker cell and position the ferrite plate in front of the sample to measure the co-polar signal, $Tco(\nu)$.
5. Manually rotate the receiving horn H2 (together with the frequency-extender module), by 90° to measure the cross-polar signal, $Tcr(\nu)$.
6. Use (4) to calculated RHCP and LHCP and obtain the CD spectrum by (5).

Scheme 1 will invariably introduce significant systematic errors. Further, random error is introduced as cables suffer movement away from how they lay during calibration. To avoid such errors, scheme 2 has been devised. It introduces a 45° wire-grid polarizers between F4 and H2 that, with a pair of settings, is used to obtain an equivalent measure of the cross-polar signal component (as is shown Fig. 3). A Jones' analysis shows that the linearly-polarized signal at 45° from x-axis, T_{45}, is composed of a mixture of the horizontal and vertical components:

$$T_{45}(\nu) = \frac{1}{\sqrt{2}}\left(Tcr(\nu) + Tco(\nu)\right). \quad (6)$$

To determine the cross-polar signal, we rewrite (6) as

$$Tcr(\nu) = \sqrt{2}T_{45}(\nu) - Tco(\nu)\,. \quad (7)$$

The advantage of this equivalent procedure for determination of cross-polarisation is that cables and receive-horn remain untouched, hence no introduction of phase-noise and anulling of calibration. Co-and cross-polarisation transmission are used in post processing analyses to construct L- and RHCP transmittances. Scheme 2 follows:

1. Repetition of steps 1 to 3 of scheme 1 to acquire the co-polar measurement.
2. Remove the sample and ferrite plate from position S and clean the Bruker cell with distilled water.
3. Place the empty cell at position S and the 45° wire-grid polarizer in position G1, as in Fig. 3, and re-set the background signal.
4. Inject liquid sample into the cell and position the ferrite plate in front of the sample to make $T_{45}(\nu)$ measurement.
5. Use $Tco(\nu)$ and $T_{45}(\nu)$ to calculate $Tcr(\nu)$ with (7) and obtain CD spectrum by equations (4) and (5).

Figs. 4 and 5 compare the two measurement schemes for a pH 7, 5mg/ml Myoglobin liquid sample over D and H waveguide bands. From both figures, the derived cross-polar signals (scheme 2) have been enhanced by the ferrite in order to aid computation of the CD spectrum, with stable values for 'zero-crossings' resulting. Both figures have demonstrated that rotating the receiving horn (and necessarily with it the frequency-extender module), has introduced signal loss and error. At D and H bands, the power loss and difference in absorption between both schemes introduced a frequency shift at each zero-crossing point. Comparison of schemes 1 and 2 demonstrates that the cross-polar signal can be more reliably obtained by $Tco(\nu)$ and $T_{45}(\nu)$ yielding safer CD spectrum. Scheme 2 is much easily to setup. Moreover, step 5 in scheme 1 needs to manually reconnect cables and recalibrate background signal. Signal loss and error then occur, especially at D band.

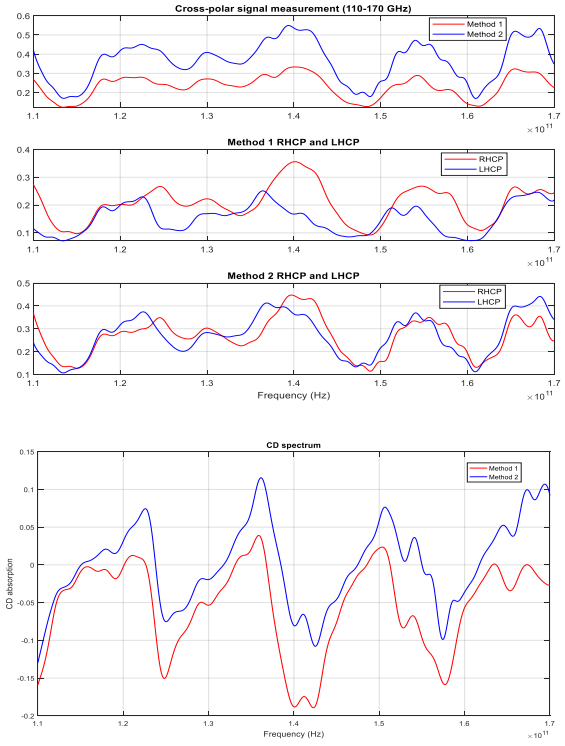

Figure 4: D band response from Schemes 1 and 2. The upper plot shows the traditional and synthesised cross-polar signals. The second and the third plots show the right-hand and left hand circularly-polarized waves of methods 1 and2. The last plot shows the comparison of CD spectra.

This article has been accepted for publication in a future issue of this journal, but has not been fully edited. Content may change prior to final publication. Citation information: DOI 10.1109/TTHZ.2020.2985642, IEEE Transactions on Terahertz Science and Technology

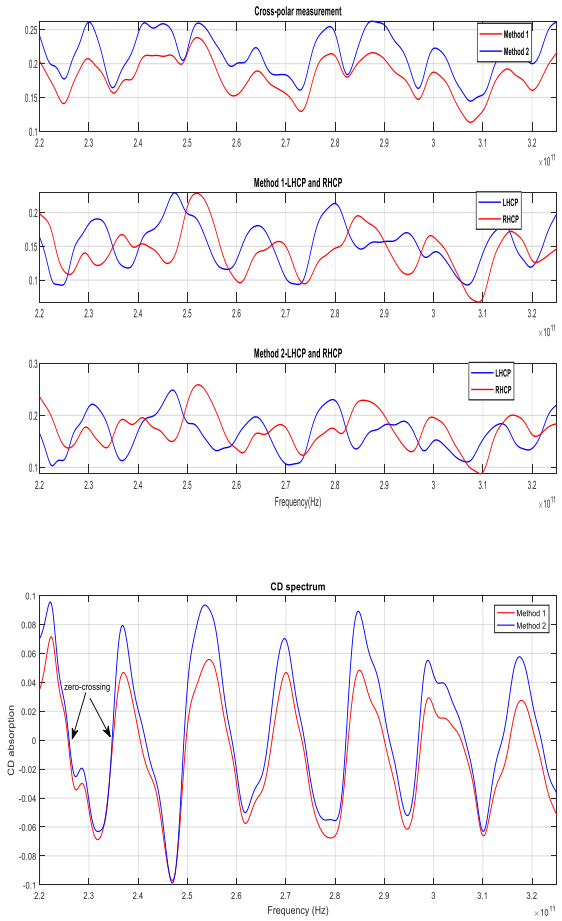

Figure 5: H band response from Schemes 1 and 2. The upper plot shows the traditional and synthesised cross-polar signals. The second and the third plots show the right- and left-hand circularly-polarized waves of schemes 1 and 2. The last plot shows comparison of CD spectra.

III. Results

A. The Far-UV CD spectrum

Far-UV CD spectroscopy is used to independently establish the conformational state of protein secondary structure and thereby interpret sub-THz CD spectra. While far UV CD is sensitive to high-energy activity of side-chain functional groups, sub-THz CD will contrariwise be responding to low-energy, group-vibrational modes of the whole backbone of the long-chain molecule. Far-UV CD spectra of Myoglobin in 20 mM phosphate buffer at pH 8.26, pH 7, and pH 5.5, are shown in Fig. 6. The sample thickness is 0.5 mm. UV CD absorption measurement is based on the Beer–Lambert law. The relationship of absorbance, concentration, and cuvette path length can be written as

$$A = \varepsilon \times l \times c \tag{8}$$

where ε is molar extinction coefficient, l is path length, and c is sample concentration. Concentration level and path length of cuvette are critical in the UV CD measurement. Normally, for secondary structure study (180-250 nm), 0.1 mg/ml of samples is recommended in 1 mm path length of cuvette. The MB solutions were diluted from the 5mg/ml Myoglobin samples which were used on THz CD QO system in same day. The three spectra show one peak at 192 nm and two troughs at 209 nm and 222 nm. They indicate that the conformation of MB over the three buffer states are α-helix, meaning the protein is stable in those buffers. The diminishing peak at 192 nm and rising features at 209 nm and 222 nm, indicate the influence of pH. When dissolving MB in the buffer below pH 2.5, the strength of H-bonds between the heme group and main chain is weaker and begins to deteriorate. When using buffers of higher or lower pH value relative to neutral, secondary structure will denature into random coils. Although Far-UV CD spectra show clear curves that are directly linked to the protein secondary structure, it is sensitive to sample concentration and significantly influences absorption readings. For MB measurement, concentrations exceeding 0.25 mg/ml reduces S/N for wavelengths longer than 200 nm.

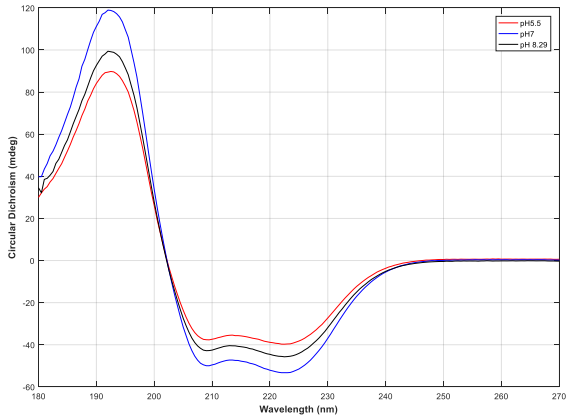

Figure 6: Far-UV CD spectrum of Myoglobin in 20 mM phosphate buffer with pH 5.5 (red), pH 7 (blue), and pH 8.26 (black).

B. Sub-THz CD spectrum

From the comparisons of schemes 1 and 2 above, 2 is to be preferred. All following discussion now concerns scheme 2. The spectral locations of CD zero-crossings are now given to identify samples by acting as their biological finger print or 'barcode'. Shifts in zero-crossings result from conformational reconfiguration in the secondary structure of the protein in response to its variations in the state of its environment (e.g. pH, buffer concentration etc). Again, while shorter x-ray and UV wavelengths of light probes the action of light side-chain molecules, longer wavelength THz light probes lower-energy action associated with molecular rotation and coupled-vibrational modes [41]. Such activity of the secondary structure of a protein makes its CD spectrum a unique encoding or register of its condition.

In Fig.7 the red line represents the free-space CD spectrum. Thirteen zero-crossing are noted for the empty cell (whose window materials are the ultra low-loss TPX, $100\mu m$ air space between two TPX windows). Different samples induce different levels of absorption of the circularly-polarized wave culminating in different degrees of shift at each zero-crossing point relative to the empty-cell calibration. The THz CD spectrum of the empty cell is dominated by the ferrite plate. Since the sample holder is extremely low-loss and not comprised of an optically-active material, it will not couple to the circularly polarized wave, and so can be considered to establish a free-space CD spectrum. Water, being achiral, is insensitive to the circularly polarized light. Filling the

This article has been accepted for publication in a future issue of this journal, but has not been fully edited. Content may change prior to final publication. Citation information: DOI 10.1109/TTHZ.2020.2985642, IEEE Transactions on Terahertz Science and Technology

sample-holder with pure water yields a similar THz CD spectrum comparing with the empty cell. The reduced amplitude reading for the water CD spectrum follows from water absorption by component co- and cross-polar transmission waves. Significantly, the zero-crossings remain statistically invariant. The thickness of the sample solution is adjusted to be 100 μm. This as a compromise between optimum beam-sample-interaction and S/N. However, by dissolving MB proteins into the buffer (black line in Fig.7), secondary structures of MB show absorption by interacting with the component orthogonal linear polarisations that comprise the THz circularly polarized wave, inducing shifts in where zero-crossings occur. The spectrum of zero-crossings may be regarded as a THz CD bio-signature of MB proteins.

Before comparing the samples at different pH values of buffer and concentrated level, the repeatability and stability of measurements is tested. Fig. 8 provides comparison of three CD spectra of pH 7 5mg/mL Myoglobin from three independent measurements. Test 1 are measurements from a given day. Test 2 and 3 are subsequent measurements on a later day. Test 1 with respect to tests 2 and 3 has an RMS error of 2 and 2.14, respectively. Tests 2 and 3 have RMS error of 0.32. Since the system needed to be re-calibrated, test 2 and test 3 show the smaller error. All the measurements in Fig. 10 and 11 were done in one day to reduce the error. In each measurement, the Brucker cell was washed in doubly-distilled water and refilled with new sample to ensure the stability. The measurement procedure followed steps 1 to 4. The sensitivity of the system to samples with a concentration from 0.25 to 5 mg/mL need to be tested. Sushko et al [39], demonstrated that the concentration sensitivity of MB fell from 0.25 to 100 mg/ml in sub-TH range. Since the ferrite plate is integral to the measurement process, it is important to test if the system is still sensitive to low sample concentration when introducing the ferrite plate into the transmission measurement path. The S_{21} plot in Fig. 9 shows that the system is capable of tracking the difference between each concentration level.

According to far-UV CD spectra, pH values serve as a key parameter in influencing MB secondary structure and its CD absorption reading. The spectra in Fig. 6 show the absorption at the first peak drops from 120 to 99 (pH 8.26) and 89 (pH 5.5), respectively. The peak at pH 5.5 also shifts from 192 nm to 192.5 nm. The drop in absorption at 192, the spiked reading at 209 nm and 222 nm, and the frequency shift all suggest that the pH value has begun to influence hydrogen bonding inside the folded MB, especially for the buffer with pH 5.5. Figs. 10 and 11 show the influence of pH values for three different groups of MB liquid samples over D- and H-band. The pure phosphate buffers suffer the worst phase-noise at D-band. This phenomenon indicates that more obvious frequency shifts between the zero-crossing points in the D band are expected. The CD spectra of 5mg/ml, 1mg/ml, and 0.25mg/ml groups show signs of noise > 150 GHz which are caused by the buffer absorption. By increasing the concentration of MB protein, the influence of water absorption is muted and provides seven zero-crossing events in 5mg/ml group. However, for 1mg/ml and 0.25mg/ml noise becomes significant between 153 and 159 GHz due to heavy signal attenuation by water.

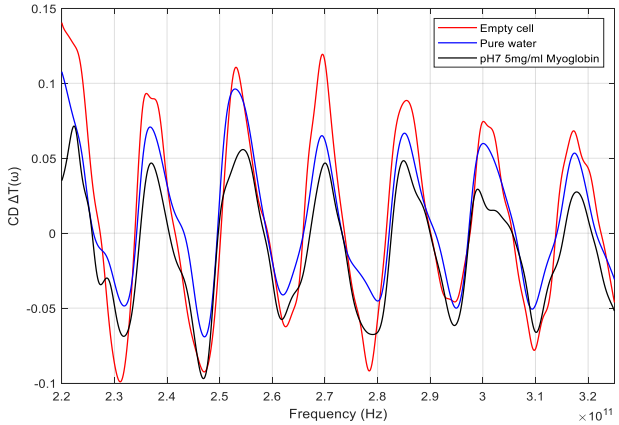

Figure 7 CD spectrum of: empty cell (red); pure water (blue); and, pH7 5mg/ml the Myoglobin sample (black).

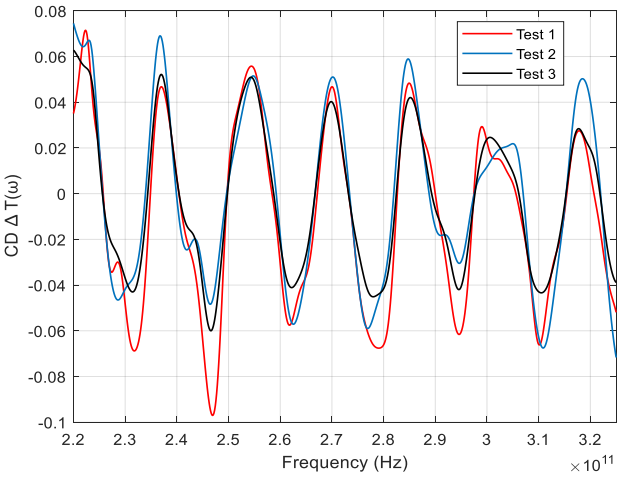

Figure 8: Four separated CD measurements of pH 7 5mg/mL of Myoglobin for testing the repeatability and errors. In each measurement, the cell was cleaned by pure water and refilled with new sample.

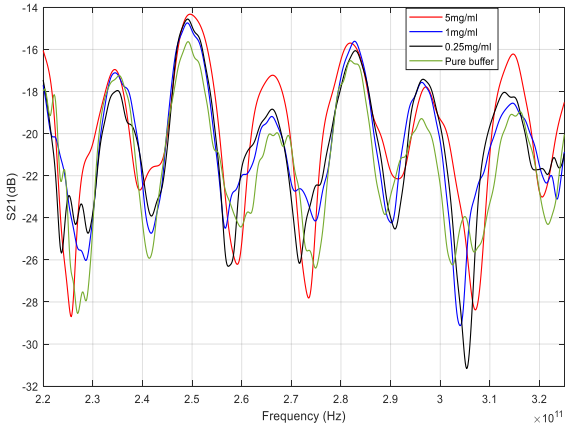

Figure 9: S_{21} plots for pH 7 Myoglobin in 5 mg/mL (red), 1 mg/mL (blue), 0.25 mg/ml (black), and pure pH7 buffer (green) for testing the system sensitivity to low sample concentration.

Each zero-crossing point suffers a frequency shift on average in the groups of 1mg/ml and 0.25mg/ml, their CD spectra approaching that for the pure buffer. In comparison

This article has been accepted for publication in a future issue of this journal, but has not been fully edited. Content may change prior to final publication. Citation information: DOI 10.1109/TTHZ.2020.2985642, IEEE Transactions on Terahertz Science and Technology

with far-UV CD spectra in Fig. 6, pH values of 8.26 and 5.5 slightly reduce the CD reading by influencing hydrogen bonds inside the folding MB. As noted above, a large number of water molecules replaced by MB proteins is critical, as such replacement reduces interaction with water molecules and enable more accurate data collection in the sub-THz CD measurement. Here we analyse the sub-THz CD spectra for 5mg/ml, which provides the most stable and clear reading of zero-crossing points which have minimal variation, making this sub-THz CD spectra more reliable when used to track bio-molecular response to its environment. As expected, the comparison of CD spectra in the 5mg/ml group exhibits large frequency shifts occurring at the 2nd (122.9 -123.8 GHz), 4th (137.9- 138.5 GHz), 5th (147.5- 149.1 GHz), 6th (153.1- 155 GHz), and 7th (161.7- 163.3 GHz) zero-crossing points at D band. The 4th and 6th zero-crossing points for pH 8.26 and pH 5.5 MB samples in both UV and sub-THz CD indicate that the strength of hydrogen bonds inside the proteins' secondary structure have been impacted as aforementioned.

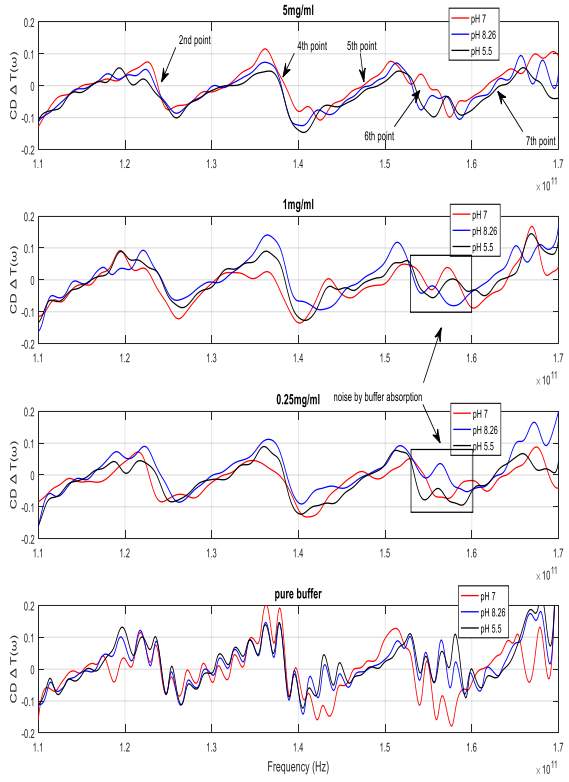

Figure 10: Comparisons of sub-THz CD spectra with different pH values at D band (110 – 170 GHz). The concentration level from first to the third plots are 5mg/ml, 1mg/ml, and 0.25mg/ml, respectively. The last plot shows the comparison with pure phosphate buffer with different pH values.

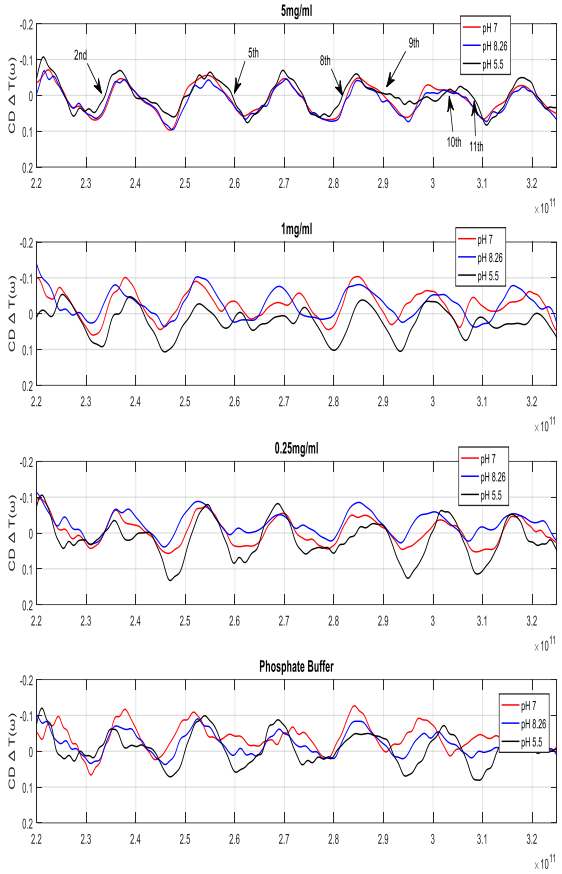

Figure 11: Comparisons of sub-THz CD spectra with different pH values in H band (220 – 325 GHz). The concentration level from first to the third plots are 5mg/ml, 1mg/ml, and 0.25mg/ml. The last plot shows the comparisons pure phosphate buffer with different pH values.

H-band exhibits similar sub-THz CD to D-band (see Fig. 11). The sub-THz CD spectra for 1mg/ml and 0.25mg/ml MB samples are similar to the CD spectra of the pure buffers and have obvious frequency shifting of greater than 1 GHz at each of the zero-crossing points. The spectrum lying between 220 to 230 GHz is strongly affected by the buffer absorption and introduces noise. The influence of buffer absorption is mitigated by raising the level of concentration to 5mg/ml, resulting in 13 zero-crossing points. From the previous description for far-UV CD spectroscopy, pH 5.5 buffer has a stronger influence over the MB secondary structure. At H band, such an influence contributes to obvious frequency shifts at the 2nd (233.8 -234.9 GHz), 5th (258.2 -259.5 GHz), 8th (281.7-283.1 GHz), 9th (288.9- 291.8 GHz), 10th (297.4- 302 GHz), and 11th (305.5 -307.7GHz) zero-crossing points comparing to that of the pH 7 and pH 8.26 MB solutions. However, the drop of CD reading of pH 5.5 MB solution between 290 to 310 GHz causes shifting at 9th (290 -292 GHz), 10th (297 -302 GHz), and 11th (305.5 -308.7 GHz) points. It indicates that MB dissolves more readily in pH 7 and pH 8.26 phosphate buffers. Although sub-THz CD spectra shows the secondary structures of MB remains α-helix for pH 5.5, pH values of 5.5 and lower, as described in section A, are not native circumstances for MB

proteins. By juxtaposing the spectra of pH 7 and pH 8.26 MB solution, the frequency shifts at 250, 290, and 297 GHz become more pronounced. The three noticeable frequency shifts indicate that MB secondary structures are also influenced by pH 8.26 buffers, although not as strong as the solutions for the lower pH values. The positions of all zero-crossing points for 5mg/ml MB in pH 8.26, 7, and 5.5 at D and H bands are shown in table 1 and 2.

The reduced absorption rate at 192, increased values at 209 nm and 222 nm, and frequency shift all suggest that the pH value has begun to influence hydrogen bonds inside the folding MB, especially in buffer with pH 5.5. Similar phenomenon is also observed in Fig. 10 and Fig. 11, showing pH 5.5 MB sample reporting a more obvious shift than its pH 8.26 MB counterpart. The Far-UV CD spectra from Fig.6 have demonstrated that MB is extremely stable when dissolved in these buffers (α-helix**)**, leading more reliability of sub-THz CD signatures. The Sub-THz CD signatures remain stable even for samples of higher levels of concentration. The highly solvated samples are also measured for biological spectral reading. By measuring proteins and finding their specific sub-THz CD signatures, a database can be constructed to understand the conformational space of proteins and provide insight into the low-energy modes of co-operative vibrations as well as their role in metabolic functions.

Table 1. Positions of zero-crossing points for 5mg/ml in D band

Zero crossing	GHz (at pH 8.26)	GHz (at pH 7.00)	GHz (at pH 5.50)
1st	116.05	115.07	116.10
2nd	123.80	123.46	122.90
3rd	132.00	131.77	132.20
4th	138.02	138.50	137.90
5th	148.25	147.50	149.10
6th	153.10	155.00	153.40
7th	162.55	161.70	163.33

Table 2. Positions of zero-crossing points for 5mg/ml in H band

Zero crossing	GHz (at pH 8.26)	GHz (at pH 7.00)	GHz (at pH 5.50)
1st	225.6	225.65	225.7
2nd	234.9	234.65	233.8
3rd	240.5	240.4	239.6
4th	250.87	249.7	250.6
5th	258.2	258.4	259.46
6th	267.3	267.2	266.9
7th	273	273.2	273.76
8th	283.1	282.65	281.7
9th	288.9	290	291.8
10th	298.17	297.4	302
11th	305.5	305.5	308.7
12th	315.7	315.45	315.2
13th	320.5	320.7	320.95

IV. Conclusion

A sub-THz Circular Dichroism Quasi-Optical spectrometer operating over the waveguide bands 110 to 170 GHz and 220 to 325 GHz is introduced. Conventional far-UV CD spectroscopy was used to independently ascertain the secondary structure of Myoglobin. Sub-THz QO CD spectroscopy is aided by the inherent signal and beam conditioning efficiency that is characteristic of quasi-optical circuits and promotes simple sample-handling leading to highly repeatable CD signatures in the study of a proto-typical protein, Myoglobin, with buffers of various concentrations at different pH values. Furthermore, the challenge of working with water-soluble samples was addressed. Though CD is insensitive to water which is achiral, the path-length for the THz probe-beam must be optimized to retain a workable dynamic range to avoid the problem of water absorption. In contrast, far-UV CD spectroscopy suffers noise when the concentration level of a sample is too high. For far-UV CD, a 5 mg/ml Myoglobin solution reports a S/N < 1 for wavelengths longer than 220 nm. However, in the sub-THz CD QO system, the spectra shows that higher concentrations aid in securing more stable spectra across both frequency bands tested. So in comparison to far-UV CD spectroscopy, a highly concentrated sample only aids the measurement process. While the initial trials of sub-THz CD QO spectroscopy seem to be suited for liquid biological samples, much supplementary data is required to construct a comprehensive database of solvated bio-molecular logical.

References

[1] D. Turton, H. Senn, T. Harwood, A. Lapthorn, E. Ellis and K. Wynne, "Terahertz underdamped vibrational motion governs protein-ligand binding in solution", *Nature Communications*, vol. 5, no. 1, 2014.

[2] F. Novelli et al., "Time-Domain THz Spectroscopy Reveals Coupled Protein–Hydration Dielectric Response in Solutions of Native and Fibrils of Human Lysozyme", *The Journal of Physical Chemistry B*, vol. 121, no. 18, pp. 4810-4816, 2017.

[3] Xu, J., Plaxco, K. and Allen, S. (2006). Probing the collective vibrational dynamics of a protein in liquid water by terahertz absorption spectroscopy. *Protein Science*, 15(5), pp.1175-1181.

[4] Xu, J., Plaxco, K. and Allen, S. (2006). Collective Dynamics of Lysozyme in Water: Terahertz Absorption Spectroscopy and Comparison with Theory. *The Journal of Physical Chemistry B*, 110(47), pp.24255-24259.

[5] P. Siegel, "Terahertz Technology in Biology and Medicine", *IEEE Transactions on Microwave Theory and Techniques*, vol. 52, no. 10, pp. 2438-2447, 2004.

[6] E. Pickwell, B. Cole, A. Fitzgerald, M. Pepper and V. Wallace, "In vivo study of human skin using pulsed terahertz radiation", *Physics in Medicine and Biology*, vol. 49, no. 9, pp. 1595-1607, 2004..

[7] T. Luong, P. Verma, R. Mitra and M. Havenith, "Do Hydration Dynamics Follow the Structural Perturbation during Thermal Denaturation of a Protein: A Terahertz Absorption Study", *Biophysical Journal*, vol. 101, no. 4, pp. 925-933, 2011.

[8] Bahar, I., Lezon, T., Bakan, A. and Shrivastava, I. (2010). Normal Mode Analysis of Biomolecular Structures: Functional Mechanisms of Membrane Proteins. *Chemical Reviews*, 110(3), pp.1463-1497.

[9] Alexandrov, V. (2005). Normal modes for predicting protein motions: A comprehensive database assessment and associated Web tool. *Protein Science*, 14(3), pp.633-643.

[10] N. Tan, R. Li, P. Bräuer, C. D'Agostino, L. Gladden and J. Zeitler, "Probing hydrogen-bonding in binary liquid mixtures with terahertz time-domain spectroscopy: a comparison of Debye and absorption analysis", *Physical Chemistry Chemical Physics*, vol. 17, no. 8, pp. 5999-6008, 2015.

[11] A. Markelz, "Terahertz Dielectric Sensitivity to Biomolecular Structure and Function", *IEEE Journal of Selected Topics in Quantum Electronics*, vol. 14, no. 1, pp. 180-190, 2008.

[12] A. G. Markelz, J. R. Knab, J. Y. Chen, and Y. He, "Protein dynamical transition in terahertz dielectric response," Chem. Phys. Lett., vol. 442, pp. 413–417, 2007.

[13] J.-Y. Chen, J. R. Knab, S. Ye, Y. He, and A. G. Markelz, "Terahertz dielectric assay of solution phase protein binding," Appl. Phys. Lett., vol. 90, pp. 243901-1–243901-3, 2007.

[14] J. Neu and M. Rahm, "Terahertz time domain spectroscopy for carrier lifetime mapping in the picosecond to microsecond regime", *Optics Express*, vol. 23, no. 10, p. 12900, 2015.

[15] K. Lien Nguyen, T. Friščić, G. Day, L. Gladden and W. Jones, "Terahertz time-domain spectroscopy and the quantitative monitoring of mechanochemical cocrystal formation", *Nature Materials*, vol. 6, no. 3, pp. 206-209, 2007.

[16] R. Falconer and A. Markelz, "Terahertz Spectroscopic Analysis of Peptides and Proteins", *Journal of Infrared, Millimeter, and Terahertz Waves*, vol. 33, no. 10, pp. 973-988, 2012. H. Vondracek, J. Dielmann-Gessner, W. Lubitz, M. Knipp and M. Havenith, "THz absorption spectroscopy of solvated β-lactoglobulin", *The Journal of Chemical Physics*, vol. 141, no. 22, pp. 22D534, 2014.

[17] C. Reid, G. Reese, A. Gibson and V. Wallace, "Terahertz Time-Domain Spectroscopy of Human Blood", *IEEE Transactions on Terahertz Science and Technology*, vol. 3, no. 4, pp. 363-367, 2013.

[18] M. Woerner, W. Kuehn, P. Bowlan, K. Reimann and T. Elsaesser, "Ultrafast two-dimensional terahertz spectroscopy of elementary excitations in solids", *New Journal of Physics*, vol. 15, no. 2, p. 025039, 2013.

[19] O. Sushko, R. Dubrovka and R. Donnan, "Terahertz Spectral Domain Computational Analysis of Hydration Shell of Proteins with Increasingly Complex Tertiary Structure", *The Journal of Physical Chemistry B*, vol. 117, no. 51, pp. 16486-16492, 2013.

[20] R. Singh, D. George, C. Bae, K. Niessen and A. Markelz, "Modulated orientation-sensitive terahertz spectroscopy", *Photonics Research*, vol. 4, no. 3, p. A1, 2016.

[21] C. Mattos, "Protein–water interactions in a dynamic world", *Trends in Biochemical Sciences*, vol. 27, no. 4, pp. 203-208, 2002..

[22] S. Kelly, T. Jess and N. Price, "How to study proteins by circular dichroism", *Biochimica et Biophysica Acta (BBA) - Proteins and Proteomics*, vol. 1751, no. 2, pp. 119-139, 2005.

[23] Anshuman Kumar, Reinhard Schweitzer-Stenner, and Bryan M. Wong, "A New Interpretation of the Structure and Solvent Dependence of the far UV circular Dichroism Spectrum of Short Oligopeptide", *Cehm. Commun., 2019, 55, 5701.*

[24] Böhm, G., Muhr, R., & Jaenicke, R. (1992). Quantitative analysis of protein far UV circular dichroism spectra by neural networks. *"Protein Engineering, Design and Selection", 5*(3), 191–195.

[25] Nagy, G., Igaev, M., Jones, N. C., Hoffmann, S. V., & Grubmüller, H. (2019). SESCA: Predicting Circular Dichroism Spectra from Protein Molecular Structures. *Journal of Chemical Theory and Computation*, *15*(9), 5087–5102.

[26] S. Kelly and N. Price, "The Use of Circular Dichroism in the Investigation of Protein Structure and Function", *Current Protein & Peptide Science*, vol. 1, no. 4, pp. 349-384, 2000.

[27] B. Wallace, "Using Circular Dichroism (CD) and Synchrotron Radiation Circular Dichroism (SRCD) Spectroscopy to Study Membrane Proteins", *Biophysical Journal*, vol. 98, no. 3, pp. 209a-210a, 2010.

[28] D. Kurouski, "Advances of Vibrational Circular Dichroism (VCD) in bioanalytical chemistry. A review", *Analytica Chimica Acta*, vol. 990, pp. 54-66, 2017.

[29] G. Magyarfalvi, G. Tarczay and E. Vass, "Vibrational circular dichroism", *Wiley Interdisciplinary Reviews: Computational Molecular Science*, vol. 1, no. 3, pp. 403-425, 2011.

[30] Choi, W.J., Cheng, G., Huang, Z. *et al*. Terahertz circular dichroism spectroscopy of biomaterials enabled by kirigami polarization modulators. *Nat. Mater.* **18,** 820–826 (2019).

[31] Sun, B. and Yu, Y. (2018). Analysis of circular dichroism in chiral metamaterial at terahertz frequencies. *Journal of Physics D: Applied Physics*, 52(2), p.025105.

[32] Jing Xu, Jhenny Galan, Gerry Ramian, Pavlos Savvidis, Anthony Scopatz, Robert R. Birge, S. James Allen, Kevin Plaxco, "Terahertz Circular Dichroism Spectroscopy of Biomolecules", Nov. 2003.

[33] P. Polavarapu and C. Zhao, "Vibrational circular dichroism: a new spectroscopic tool for biomolecular structural determination", *Fresenius' Journal of Analytical Chemistry*, vol. 366, no. 6-7, pp. 727-734, 2000.

[34] J. Choi and M. Cho, "Terahertz Chiroptical Spectroscopy of an α-Helical Polypeptide: A Molecular Dynamics Simulation Study", *The Journal of Physical Chemistry B*, vol. 118, no. 45, pp. 12837-12843, 2014.

[35] B. Yang and R. Donnan, "Enhanced rapid and accurate sub-THz magneto-optical characterization of hexaferrite ceramics", *Journal of Magnetism and Magnetic Materials*, vol. 323, no. 15, pp. 1992-1997, 2011.

[36] B. Yang, R. Wylde, D. Martin, P. Goy, R. Donnan and S. Caroopen, "Determination of the Gyrotropic Characteristics of Hexaferrite Ceramics From 75 to 600 GHz", *IEEE Transactions on Microwave Theory and Techniques*, vol. 58, no. 12, pp. 3587-3597, 2010.

[37] Laman, N., Harsha, S., Grischkowsky, D. and Melinger, J. (2008). High-Resolution Waveguide THz Spectroscopy of Biological Molecules. *Biophysical Journal*, 94(3), pp.1010-1020.

[38] Zhang, C. and Durbin, S. (2006). Hydration-Induced Far-Infrared Absorption Increase in Myoglobin. *The Journal of Physical Chemistry B*, 110(46), pp.23607-23613.

[39] Sushko, O., Dubrovka, R. and Donnan, R. "Sub-terahertz spectroscopy reveals that proteins influence the properties of water at greater distances than previously detected" [J. Chem. Phys. 142, 055101 (2015)].

[40] R. Lewis, *Terahertz physics*. Cambridge: Cambridge University Press, 2012.

[41] C.R. Nave, "Interaction of radiation with Matter", Georgia State University, *Hyperphysics.phy-astr.gsu.edu*, 2016.

Jhih-Hong Cheng received the B.S. degree in Electronic Engineering from Chien Hsin University of Science and Technology, Taiwan in 2012 and the M.S. degree in Electrical & Computer Engineering from University of Colorado, Colorado Springs, USA in 2014. He is currently pursuing the Ph.D. degree in Electronic Engineering & Computer Science at Queen Mary, University of London, UK. His research interest includes biological application in THz band using quasi-optical system and time-domain spectroscopy, and RFID antenna design in ultra-high frequency band

Robert Jones received the MEng (Hons.) degree in Electronic Engineering and Telecommunications from Queen Mary University of London in 2017. He is currently pursuing the Ph.D degree in the Antennas and Electromagnetics group, Queen Mary University of London. His research interests include THz applications in biology.

Oleksandr Sushko received the M.Sc. (Hons.) degree in radio-engineering from National Technical University of Ukraine "Kyiv Polytechnic Institute" in 2010, and the Ph.D. degree from Antennas and Electromagnetics Group, Queen Mary University of London in 2014. He was a Post-Doctoral Research Assistant with the Antennas and Electromagnetics Group, Queen Mary University of London, where he was involved in the development of millimeter-wave components for new generation of space-born sounder for meteorological satellite, then on the development of quasi-optical sub-THz sources-based arrays of Schottky diodes. Currently he is a lecturer at Radio engineering Faculty of National Technical University of Ukraine "Igor Sikorsky Kyiv Polytechnic Institute." Dr. Sushko has authored and co-authored more than 30 journal and conference papers. His current research interests include satellite communications, microwave, millimeter-wave and THz antennas and components, quasi-optical circuits and their applications.

Yumiko Tashiro received the B.Sc. (Hons.) in biochemistry from University of Leeds, UK, the M.Sc.in plant genetic manipulation from University of Nottingham, UK, and the M.Phil. in biochemistry from Queen Mary, University of London, UK .
She is currently a biochemistry laboratories manager in School of Biological and Chemical Sciences, Queen Mary, University of London, UK and support several research projects. Her researches interest include the application of instrumental techniques for the determination of protein structure and function in structural biology.

Robert Donnan received his Ph.D. (Solid State Physics) in 2000 from the University of Wollongong, NSW, Australia. Under an EPSRC contract in 2001, he commenced as a post doctoral research assistant in the Department of Electronic Engineering, Queen Mary, University of London , developing diffracted Gaussian beam optics for design-verification of quasi-optical systems. In March 2003 he was appointed to a Lectureship in the Department. His research, broadly, is in development of mm/submm-wave and THz measurement systems to serve basic and applied research in medical and structural imaging and in spectrometric studies of materials, metamaterials and biomaterials. A key aspect of this work is development of microstructured componentry requiring accurate measurements of plane-wave transmission/refelection spectra. These are used in determiantion of optical/magnetooptical constants and verifiaction of component design-performance.